Dynamic Effects on the Powder Line Shapes of Half-Integer Quadrupolar Nuclei: A Solid-State NMR Study of XO_4^- Groups

Robert W. Schurko,[†] Sungsool Wi,[‡] and Lucio Frydman*

Department of Chemical Physics, Weizmann Institute, 76100 Rehovot, Israel, and Department of Chemistry, University of Illinois at Chicago, Chicago, Illinois 60607

Received: August 6, 2001

Multinuclear solid-state nuclear magnetic resonance studies ($^{185/187}$Re, ^{55}Mn, ^{75}As, and ^{1}H NMR) were undertaken on a series of polycrystalline inorganic salts incorporating diamagnetic XO_4^- groups, X being a half-integer quadrupolar nucleus. Exploiting data acquisition protocols that were recently developed for observing undistorted half-integer quadrupole central transitions, some of the largest quadrupole coupling constants reported to date by high field NMR were characterized ($e^2qQ/h \approx 300$ MHz). On repeating such measurements as a function of temperature, certain samples displayed reversible changes that could not be rationalized in terms of the usual temperature dependencies of the nuclear quadrupolar couplings. Instead, dynamic exchange processes between chemically or magnetically inequivalent sites had to be invoked. To quantitatively analyze these processes, the semiclassical Bloch−McConnell formalism for chemical exchange was extended to account for second-order quadrupole effects. Insight into the potential nature of the chemical dynamics was also obtained from quantum chemical calculations of the coupling parameters on model systems.

1. Introduction

Nuclear magnetic resonance (NMR) offers one of the most established approaches for the detection and molecular-level characterization of dynamics in solids.[1−5] The anisotropic nature of solid NMR interactions provides well-defined local probes of orientation, and motions or chemical exchange processes yield rate-dependent changes in the experimental line shapes that can be interpreted in terms of established kinetic models. Such dynamic NMR theories were laid down decades ago for the case of first-order dipolar, chemical shielding, and quadrupolar anisotropies. In particular, variations of the classical Bloch−McConnell equations[6,7] have served as some of the most widely used tools for elucidating dynamics in biological, organic, and polymeric solids via a variety of ^{13}C, ^{31}P, and ^{2}H variable-temperature techniques.

Recent years have witnessed a surging interest in the solid-state NMR of half-integer quadrupolar nuclei.[8−13] This is partly due to methodological advances in spectral resolution and assignment techniques, as well as to the realization of the numerous contributions that this methodology can make to chemistry, materials sciences, and structural biophysics. During the course of applying such methods to a variety of molecular and biomolecular solids, we found that an important area to understand and develop in this field concerns the potential effects that dynamics may have on the spectra arising from higher half-integer nuclei. Such treatments lie at a comparatively less developed stage than their spin-$^1/_2$ and spin-1 counterparts, particularly with regards to modeling how dynamics will affect the second-order quadrupolar line shapes of central and multiple-quantum (MQ) transitions. This is somewhat of a paradox, considering that it has long been known that as a result of dynamics in the surrounding lattice, the electric field gradients (EFGs) which determine the magnitudes of quadrupolar interactions can be substantially temperature dependent.[14,15]

The present paper discusses both theoretically as well as experimentally a number of examples of how molecular motions may influence the NMR powder patterns of half-integer quadrupolar nuclei. Treatments on the effects of motions on second-order Hamiltonians were in fact discussed years ago by Luz et al.; yet the emphasis of those studies were EPR-related zero-field couplings treated with a diffusive stochastic Liouville theory.[16] As this work was being readied, two new studies appeared concerning the effects of motions on half-integer quadrupolar nuclei: a density matrix treatment by Kristensen and Farnan, which employed Liouville−von Neumann superoperators and the Cartan−Weyl algebra to simulate two- and three-site chemical exchange for static and rotating solids,[17] and a study by Eckert et al. on the dynamics of phosphate groups based on a semiclassical exchange approximation.[18] A similar method was here adopted for treating static NMR spectra dominated by second-order quadrupolar and/or first-order chemical shielding interactions. A variety of line shapes that can arise due to rotational and chemical exchange processes were thus analyzed both numerically as well as analytically, and the resulting dynamic second-order quadrupolar line shapes compared with cases dominated by anisotropic first-order effects. The insight resulting from these simulations was subsequently applied to interpret a series of wide-line static ^{55}Mn and $^{185/187}$Re static NMR spectra acquired at a variety of temperatures for a series of permanganate and perrhenate complexes with generic XO_4^- structures: $NaReO_4$, NH_4ReO_4, $AsPh_4ReO_4$, $KMnO_4$, $CsMnO_4$, and PPh_4MnO_4. These experimental studies, which evidence some of the largest quadrupolar coupling constants measured to date by solid-state NMR wide-line methods, revealed a rich variety of dynamic changes. These included a

* Corresponding author. Address: Department of Chemical Physics, Weizmann Institute of Science, 76100 Rehovot, Israel. FAX: +972-8-9344123. E-mail: lucio.frydman@weizmann.ac.il.

[†] Present Address: Department of Chemistry and Biochemistry, University of Windsor, Windsor, Ontario, Canada N9B 3P4.

[‡] Present Address: Department of Chemistry, University of California, Berkeley, CA 94720.

10.1021/jp0130214 CCC: $22.00
Published on Web 12/12/2001

linear increase of e^2qQ/h with decreasing temperature, a rare instance of a decrease in e^2qQ/h with decreasing temperature, and a variety of dynamic effects on the EFG tensors resulting from intra- and extramoiety processes occurring on the NMR time scale of the second-order anisotropy. Some of these dynamics involved unusual reorientation angles, far from the tetrahedral ones that could be expected for XO_4^- groups. To shed further light into these values, a series of ab initio calculations were carried out, which showed that exchange between such angles can in fact arise from minor lattice-imposed distortions of the XO_4^- structures away from their expected crystallographic symmetry.

2. Theory

Semiclassical Exchange Formalism. As starting point for extending the semiclassical analysis of exchange to half-integer quadrupolar nuclei, we employ the expressions resulting from average Hamiltonian theory for the NMR resonance frequencies in static solid powder spectra.[10] The relevant Hamiltonian for the exchanging quadrupole nucleus will thus be assumed:

$$H = H_Q^{(1)} + H_{CS}^{(1)} + H_Q^{(2)} \tag{1}$$

where the first- and second-order quadrupolar interactions will be expressed as

$$H_Q^{(1)} = \left[\frac{eQ}{2I(2I-1)\hbar}\right] R_{20}^{(Q)}[3I_z^2 - I(I+1)] \tag{2}$$

$$H_Q^{(2)} = \left(\frac{eQ}{2I(2I-1)\hbar}\right)^2 \frac{3}{\omega_0}\{R_{2-1}^{(Q)} R_{21}^{(Q)} I_z[4I(I+1) - 8I_z^2 - 1] + R_{2-2}^{(Q)} R_{22}^{(Q)} I_z[2I(I+1) - 2I_z^2 - 1]\} \tag{3}$$

with $\{R_{2m}^{(Q)}\}_{m=0,\pm1,\pm2}$ being the orientational-dependent spherical terms transforming the interaction from its own principal axis system (PAS) into the laboratory frame. The chemical shielding is only considered up to first-order by the Hamiltonian

$$H_{CS}^{(1)} = \left[\sigma_{iso}\omega_o + \frac{2}{\sqrt{6}} R_{20}^{(CS)} B_o\right] I_z \tag{4}$$

where σ_{iso} is the isotropic chemical shielding and $R_{20}^{(CS)}$ now refers to the shielding as transformed from its own PAS. Furthermore, if only the central (or other $-m \leftrightarrow +m$) transitions are considered, first-order quadrupolar interactions can be neglected due to their I_z^2-type dependence, and the relevant evolution frequency simply becomes

$$\omega_{1/2\leftrightarrow -1/2} = \sigma_{iso}\omega_o + \frac{2}{\sqrt{6}} B_o R_{20}^{(CS)} + \frac{6}{\omega_0} C_Q^2[4I(I+1) - 3][2R_{2-1}^{(Q)} R_{21}^{(Q)} + R_{2-2}^{(Q)} R_{22}^{(Q)}] \tag{5}$$

where $eqC_Q = \chi_Q = [e^2qQ]/[4I(2I-1)\hbar]$ defines the quadrupolar coupling frequency.

These expressions can be used for modeling the effects of chemical exchange or motion on an NMR spectrum, provided that the spatial components of $H_Q^{(2)}$ and $H_{CS}^{(1)}$ are expressed in some common molecular or lattice frame simultaneously describing all interconverting sites. We describe the Euler angle sets associated to how the various components in eq 5 transform from their PAS's into the laboratory axis system by

$$\rho_{2\pm m}^{(CS)} \xrightarrow{(\alpha',\beta',\gamma')} R_{2\pm m}^{(\lambda)}(MOL) \xrightarrow{(\varphi,\theta,0)} R_{2\pm m}^{(\lambda)}(LAB) \qquad \rho_{2\pm m}^{(Q)} \xrightarrow{(\alpha,\beta,\gamma)} R_{2\pm m}^{(\lambda)}(MOL) \tag{6}$$

Multiple exchanging sites j will thus be defined by multiple $(\alpha_j,\beta_j,\gamma_j)_{1\le j\le N}$ sets of Euler angles, whereas (φ,θ) denotes a common set of powder angles which has to be suitably integrated over the solid sphere in order to sample all orientations with respect to the B_o field. The actual transformations in eq 6 can be accomplished by means of second-rank Wigner rotation matrices;[19] for instance, for the cases relevant to this study

$$R_{20}^{(CS)} = \sum_{n=-2}^{2} D_{n0}^2(\varphi,\theta,0) \sum_{m=-2}^{2} D_{mn}^2(\alpha',\beta',\gamma')\rho_{2m}^{(CS)} = \sum_{n=-2}^{2} d_{n0}^2(\theta) \sum_{m=-2}^{2} e^{-im\alpha'} d_{mn}^2(\beta') e^{-in(\gamma'+\varphi)} \rho_{2m}^{(CS)} \tag{7a}$$

$$R_{2\pm1}^{(Q)} = \sum_{n=-2}^{2} D_{n\pm1}^2(\varphi,\theta,0) \sum_{m=-2}^{2} D_{mn}^2(\alpha,\beta,\gamma)\rho_{2m}^{(Q)} = \sum_{n=-2}^{2} d_{n\pm1}^2(\theta) \sum_{m=-2}^{2} e^{-im\alpha} d_{mn}^2(\beta) e^{-in(\gamma+\varphi)} \rho_{2m}^{(Q)} \tag{7b}$$

$$R_{2\pm2}^{(Q)} = \sum_{n=-2}^{2} D_{n\pm2}^2(\varphi,\theta,0) \sum_{m=-2}^{2} D_{mn}^2(\alpha,\beta,\gamma)\rho_{2m}^{(Q)} = \sum_{n=-2}^{2} d_{n\pm2}^2(\theta) \sum_{m=-2}^{2} e^{-im\alpha} d_{mn}^2(\beta) e^{-in(\gamma+\varphi)} \rho_{2m}^{(Q)} \tag{7c}$$

where in the quadrupolar PAS $\rho_{20} = eq/2$, $\rho_{2\pm1} = 0$, $\rho_{2\pm2} =$ and $eq\eta_Q/(2\sqrt{6})$ and in the shielding PAS $\rho_{20} = \sqrt{3/2}\delta_{CS}$, $\rho_{2\pm1} = 0$, and $\rho_{2\pm2} = \delta_{CS}\eta_{CS}/2$.

When chemical exchange occurs, the stochastic jumps that groups or molecules perform between different orientations and/or sites result in nuclear spins exchanging their local fields. Analyzing the full range of dynamic changes that will then occur in a quadrupolar NMR spectrum, from a full static condition and all the way to a fully motion-averaged resonance, is far from trivial. This is due to the interdependence of first- and second-order quadrupole effects, which will result in significant spectral changes even for central transition resonances, as the dynamic rates κ approach the second-order time scale $(\chi_Q^2/\omega_o)^{-1}$ as well as the first-order $(\chi_Q)^{-1}$ time scale. A complete description of such effects requires dealing with exchange superoperators in Liouville space; certain aspects of this formalism were recently discussed by Kristensen and Farnan, but exploring its full implications remains to be described. For the goals and needs of the present work, it will simply be assumed that exchange rates are localized in either the second-order or the first-order time scales; dynamic effects can hence be followed simply from precession frequencies such as those in eq 5 via kinetic modifications of Bloch's equations. To do so, we follow McConnell's semiclassical treatment of exchange and define, for an N-site process, an $\mathbf{M}(t)$ vector with N elements $M_j(t)$ corresponding to each of these sites' magnetizations. The equation of motion for the complete magnetization vector can then be written as[1,2,6,7]

$$\frac{d}{dt}\mathbf{M}(t) = (i\varpi + \bar{\pi})\mathbf{M}(t) \tag{8}$$

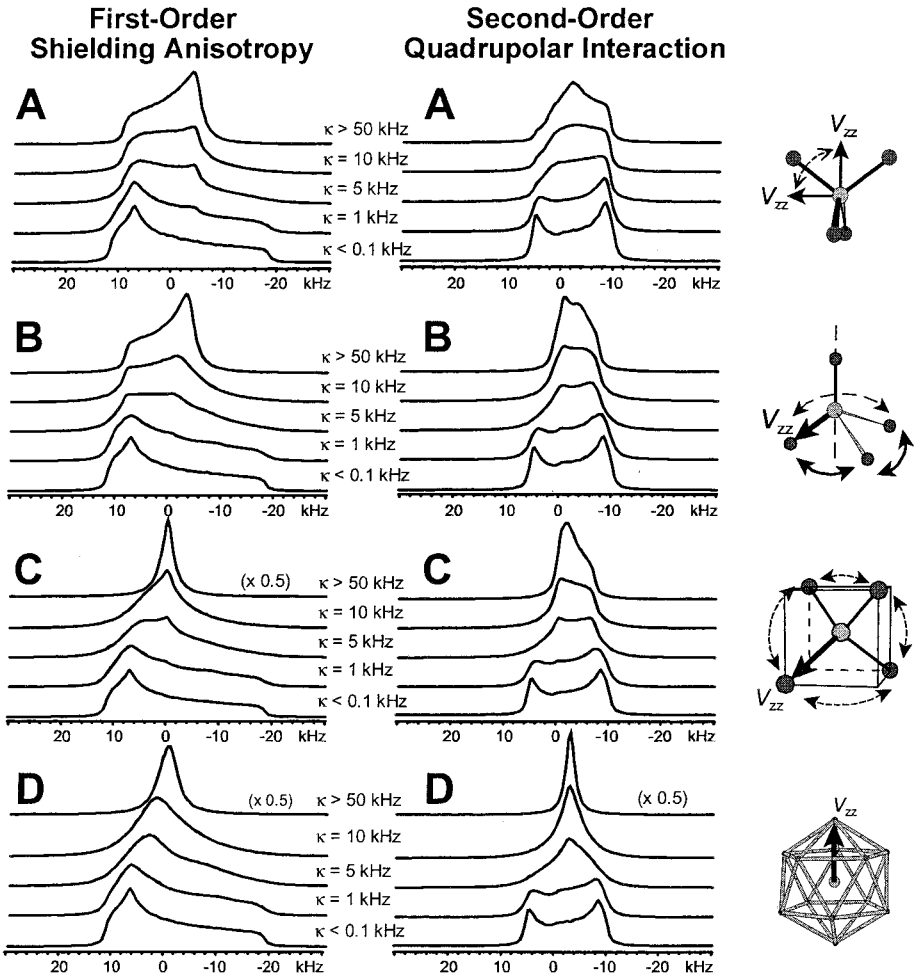

Figure 1. Comparisons between the effects introduced by different types of exchange processes on central transition line shapes affected by second-order quadrupolar vis à vis first-order shielding anisotropies. (A) Two-site exchange about orthogonal orientations. (B) Three-site reorientations about the C_3 symmetry axis of a tetrahedron. (C) Four-site exchange about the vertices of a tetrahedron. (D) Twelve-site exchange about the vertices of a dodecahedron. Besides the indicated rates κ, the following parameters were employed in the simulations: $I = {}^5/_2$, $e^2qQ/h = 6.3$ MHz, $\eta_Q = 0.1$, $\omega_o/2\pi = 85.7$ MHz (second-order line shapes); $\omega_o/2\pi = 85.7$ MHz, $\delta_{iso} = 0$ ppm, $\delta_{CS} = -324$ ppm, and $\eta_{CS} = 0.24$ (first-order patterns). As throughout the rest of this work, EFG tensor principal components are defined as $|V_{yy}| \leq |V_{xx}| \leq |V_{zz}|$, with $e^2qQ/h = eQV_{zz}$ (eQ being the nuclear quadrupole moment) and $\eta_Q = (V_{yy} - V_{xx})/V_{zz}$. Anisotropic chemical shifts are described according to $|\delta_{yy}| \leq |\delta_{xx}| \leq |\delta_{zz}|$, $\delta_{CS} = \delta_{zz}$, and $\eta_{CS} = (\delta_{yy} - \delta_{xx})/\delta_{zz}$.

Here ϖ is a diagonal matrix with elements $\omega_j + i/T_2$, ω_j being the classical precession frequency of each exchanging site and T_{2j} their respective transverse relaxation times. $\bar{\pi}$ on the other hand defines the topology and rates of the exchange process. Equation 8 can be formally solved as

$$\mathbf{M}(t) = \exp[(i\varpi + \bar{\pi})t]\mathbf{M}(t = 0) \tag{9}$$

where the initial magnetization vector is equivalent to the column vector describing the a priori probabilities for each site's occupation. The sum of magnetization from all of the sites yields an expression for the free induction decay (FID):

$$G(t) = \sum_j M_j(t) = \mathbf{1}\cdot\exp[(i\varpi + \bar{\pi})t]\cdot\mathbf{W} \tag{10}$$

where **1** is a row vector. From a computational perspective, calculating the exponential in eq 10 can be carried out by diagonalizing the non-Hermitian matrix $i\varpi + \bar{\pi}$ (for instance using the QR transformation) as

$$\mathbf{S}^{-1}(i\varpi + \bar{\pi})\mathbf{S} = \bar{\lambda} \tag{11}$$

from which $G(t)$ can be calculated with the eigenvalues λ_j:

$$G(t) = \mathbf{1}\cdot\mathbf{S}\cdot\exp[\bar{\lambda}t]\cdot\mathbf{S}^{-1}\cdot\mathbf{W} \tag{12}$$

A powder integration of such signals over polar and azimuthal (θ,φ) angles generates a final FID that when Fourier transformed yields the powder spectrum being sought. Such formalism, akin to the one recently advanced by Eckert et al,[18] was used throughout this study for analytical and numerical calculations of central transition NMR spectra. Considering other transitions and/or an additional MOL → ROTOR → LAB transformation would enable these calculations to be extended to other half-integer quadrupolar experiments such as magic-angle-spinning (MAS) and MQMAS, as will be described and illustrated elsewhere.

Prototypical Dynamic Line Shapes. It is illustrative to consider the dynamic effects that this formalism predicts for line shapes affected by first-order shielding vis à vis second-order quadrupolar interactions. Figure 1 compares the variations that can be expected from various multisite exchange processes between equally populated and chemically equivalent orientations as a function of the jump rate κ. In all cases, it is clear that the principal time scale defining the line shape changes in the order of the anisotropy involved, $\omega_o R_{20}^{(CS)}$ and χ_Q^2/ω_o for the first- and second-order interactions, respectively. Comple-

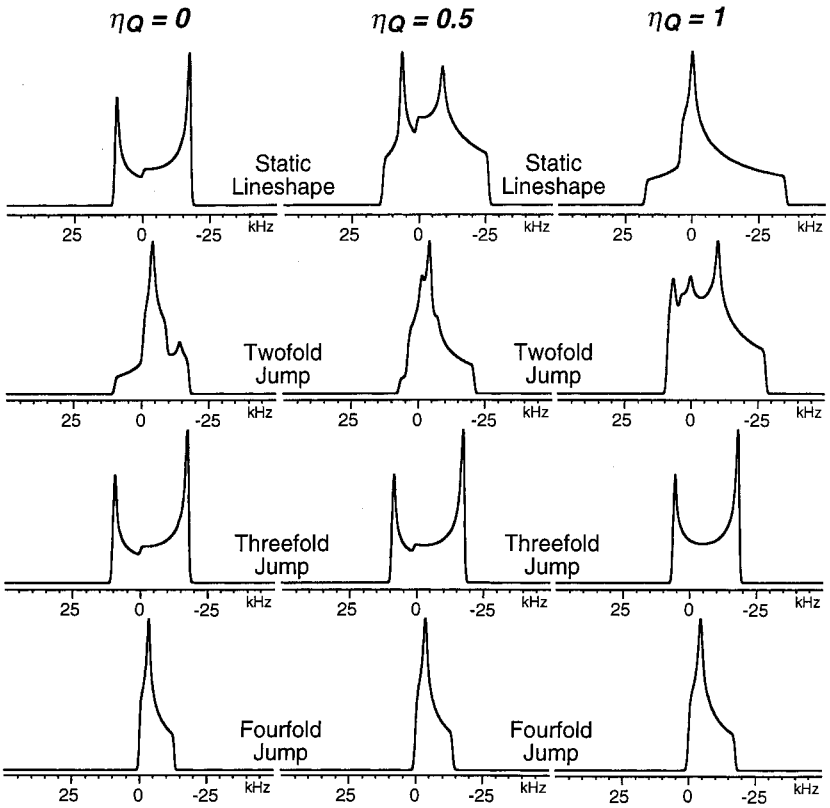

Figure 2. Comparison between the static powder patterns and limiting dynamic line shapes expected from the analytical expressions resulting from eqs 5 and 13−17 for three of the exchange models illustrated in Figure 1 (two-, three-, and four-site jump processes). All calculations assumed an $I = {}^5/_2$ site subject solely to second-order quadrupole effects with $e^2qQ/h = 10$ MHz, $\omega_o/2\pi = 114$ MHz, and the indicated η_Q values.

menting line shapes are shown in Figure 2, which compares the exchange-averaged patterns that could be analytically calculated from the formalism in the preceding paragraph for different exchange situations, with the static second-order patterns expected for a variety of asymmetry parameter values.

Analytical and numerical calculations can be most readily compared for the simplest case of a 2-fold process involving an exchange between sites related by $\pm\beta$ rotations around the z axes of their PAS's, a common type of reorientation defined by $(\alpha_1,\beta_1,\gamma_1) = (0°,\beta,0°)$, $(\alpha_2,\beta_2,\gamma 2) = (0°,\beta,180°)$. From eqs 5−7, it follows that the relevant expressions for the sites' exchanging frequencies are then

$$\omega^{(CS)}(\pm\beta) = \sigma_{iso}\omega_o + \sqrt{\frac{2}{3}}\omega_o\delta[2A(3\cos^2\theta - 1) \mp 3B\sin 2\theta\cos\varphi + 6C\sin^2\theta\cos 2\varphi] \quad (13a)$$

$$\omega^{(Q)}(\pm\beta) = \frac{6}{\omega_0}\chi_Q{}^2[4I(I+1) - 3] \times \{A^2(\cos^2\theta - 1)(9\cos^2\theta - 1) - B^2[(9\cos^4\theta - 12\cos^2\theta - 1)\cos^2\varphi + 3\cos^2\theta - 1] + C^2[(9\cos^4\theta - 10\cos^2\theta + 1)\cos^2 2\varphi + 12\cos^2\theta - 8] \mp AB(9\cos^2\theta - 5)\sin 2\theta\cos\varphi + 2AC\sin^2\theta(9\cos^2\theta + 1)\cos 2\theta \pm 3BC\sin 2\theta[(3\cos^2\theta - 1)\cos\varphi\cos 2\varphi + 2\sin\varphi\sin 2\varphi]\} \quad (13b)$$

where for each of the interactions

$$A = \frac{1}{8}\sqrt{\frac{3}{2}}(3\cos^2\beta - 1 + \eta\sin^2\beta) \quad (14a)$$

$$B = \frac{1}{12}\sqrt{\frac{3}{2}}\sin 2\beta\,(3 - \eta) \quad (14b)$$

$$C = \frac{1}{8}\sqrt{\frac{3}{2}}[3\sin^2\beta + \eta(1 + \cos^2\beta)] \quad (14c)$$

In the fast-exchange regime, when κ's magnitude is much larger than the anisotropic couplings, line shapes will be defined by the sum of all frequencies in eq 13 for $\pm\beta$. It can then be shown that whereas for the first-order couplings these average frequencies can be represented by an exchange-averaged tensor,[5] the second-order expressions lead to no such equivalent analogue. This feature arises from the different weightings with which the second- and fourth-rank anisotropic terms show up in the averaging of the higher-order interaction. Also worth remarking is the generally good agreement observed between the simulations recently introduced by Farnan, Eckert et al.[17,18] and those afforded by the semiclassical models in Figures 1 and 2.

Another common type of exchange in solids includes a 3-fold jump about a symmetry axis with pseudotetrahedral geometry, akin to that usual occurring in methyl or $-NH_3^+$ moieties. The exchange averaged components of the second-order interaction within the molecular frame will then read

$$R_{21}^{(Q)}R_{2-1}^{(Q)} = \begin{cases} -\frac{e^2q^2}{12}\left(1 - \frac{2\eta_Q}{3} + \frac{\eta_Q^2}{9}\right), & \text{for } (\alpha,\beta,\gamma) = (0°,125.3°,0°) \\ -\frac{e^2q^2}{12}\left(1 + \frac{\eta_Q}{3} + \frac{10\eta_Q^2}{36}\right), & \text{for } (\alpha,\beta,\gamma) = (120°,125.3°,0°) \\ -\frac{e^2q^2}{12}\left(1 + \frac{\eta_Q}{3} + \frac{10\eta_Q^2}{36}\right), & \text{for } (\alpha,\beta,\gamma) = (240°,125.3°,0°) \end{cases} \quad (15a)$$

and

$$R_{22}^{(Q)} R_{2-2}^{(Q)} = \begin{cases} \frac{e^2q^2}{12}\left(1+\frac{4\eta_Q}{3}+\frac{4\eta_Q^2}{9}\right), & \text{for } (\alpha,\beta,\gamma) = (0°,125.3°,0°) \\ \frac{e^2q^2}{12}\left(1-\frac{2\eta_Q}{3}+\frac{13\eta_Q^2}{36}\right), & \text{for } (\alpha,\beta,\gamma) = (120°,125.3°,0°) \\ \frac{e^2q^2}{12}\left(1-\frac{2\eta_Q}{3}+\frac{13\eta_Q^2}{36}\right), & \text{for } (\alpha,\beta,\gamma) = (240°,125.3°,0°) \end{cases} \quad (15b)$$

Figure 1 compares the line shape progression that will result from this motion as exchange rates are increased for the first-order shielding and second-order quadrupolar cases, while Figure 2 exhibits analytically derived second-order line shapes resulting in the fast exchange regime for a number of cases. As was the case for the two-site process, it is not clear that these patterns resemble those arising from a static half-integer quadrupole powder with any single set of EFG coupling parameters.

Finally, it is illustrative to consider the symmetry that needs to be achieved for a full exchange averaging of static anisotropies. For the case of a first-order interaction, it is known that in order to be averaged out, anisotropies need to be exchanging with a tetrahedral symmetry or higher. Such four-site exchange assumes a tensor centered on a tetrahedron and exchanging among the four main axes of the body, defining local Euler angles as

$$(\alpha,\beta,\gamma) = \begin{cases} (315°,54.7°,0°) \text{ for site 1} \\ (225°,125.3°,0°) \text{ for site 2} \\ (135°,54.7°,0°) \text{ for site 3} \\ (45°,125.3°,0°) \text{ for site 4} \end{cases} \quad (16)$$

The molecular frame first-order coupling components for these four sites then become $R_{20}^{(CS)}(\Omega_1) = -1/3$, $R_{20}^{(CS)}(\Omega_2) = -1/3$, $R_{20}^{(CS)}(\Omega_3) = 1/3$, and $R_{20}^{(CS)}(\Omega_4) = 1/3$, leading to a full averaging of anisotropies in the fast equipopulated exchange regime (Figure 1C, left panel). On the other hand, the molecular frame averages for the second-order couplings are $\langle R_{21}^{(Q)} R_{2-1}^{(Q)}\rangle = -e^2q^2(1 + 10\,\eta_Q^2/36)/3$ and $\langle R_{22}^{(Q)} R_{2-2}^{(Q)}\rangle = e^2q^2(1 + 13\eta_Q^2/36)/6$. These expressions are evidently different from zero and point out to another main difference between the averaging of first-order and second-order interactions: whereas fast tetrahedral motions will lead in the former to sharp isotropic resonances, they will result in second-order powder line shapes that are neither sharp nor defined by average coupling parameters (Figure 2, bottom row).[20] The reason for this is not unlike that preventing the MAS narrowing of second-order quadrupole patterns:[21] the symmetry of the motion is simply not high enough for coping with the fourth-rank anisotropies arising in second-order couplings. In contrast to this, an exchange process possessing a symmetry that is icosahedral or higher will succeed in averaging away both first- and second-order anisotropies. For instance, an equipopulated exchange among vertices of an icosahedron defined by

$$(\alpha,\beta,\gamma) = \begin{cases} (0°,0°,0°) \text{ for site 1} \\ (72(j-2)°,63.4°,0°) \text{ for site } j = 2-6 \\ (36°+72(j-7)°,116.6°,0°) \text{ for sites } j = 7-11 \\ (0°,180°,0°) \text{ for site 12} \end{cases} \quad (17)$$

will yield narrow resonance in the fast exchange regime for both $H_{CS}^{(1)}$ and $H_Q^{(2)}$ (Figure 1D). Notice, however, that in this case and until fast compared to the first-order quadrupolar coupling, the dynamics will average out the quadrupolar anisotropies but not the displacement arising from the isotropic quadrupolar shift. In this regards, the exchange process carries out an averaging of second-order couplings that is similar the one expected from fast double rotation (DOR).[21,22]

3. Experimental Section

The dynamic phenomena described in the preceding Section were explored in XO_4^- anions, in expectation that their high symmetry might allow them to undergo multi-fold rearrangements in the solid phase. Indeed two-, three- and 4-fold jumps in similar symmetry-endowed groups are well-known in organic solids. For the present study, X was chosen for observation, using the half-integer quadrupolar nuclei rhenium and manganese as the NMR targets. Rhenium possesses two $I = 5/2$ isotopes, ^{185}Re (37.1% nat. ab.) and ^{187}Re (62.9% nat. ab.), possessing some of the largest nuclear quadrupole moments in the Periodic Table (2.4 barn for ^{185}Re, 2.2 barn for ^{187}Re).[23] Because of this feature little solid NMR data is available about these nuclei, all of them arising from highly symmetric substitution environments.[24−26] In the present work, static powder $^{185/187}$Re NMR spectra were acquired on NH_4ReO_4, $NaReO_4$, and $AsPh_4ReO_4$ samples that were kindly provided to us by Prof. C. Barnes (University of Tennessee). These Re NMR spectra were acquired using protocols that have been recently described for collecting meaningful wide-line central transition data in the strong coupling regime.[27,28] These methods include suitably timed spin−echoes to overcome the effects of the spectrometer dead time, short pulse lengths and relatively weak *Rf* fields to maximize homogeneity in the excitation, and the co-addition of purely absorptive frequency-domain spectra acquired as a function of the transmitter irradiation offset. For the Re experiments, typical acquisitions parameters included 50−100 μs echo times, 1.5 μs excitation and refocusing pulses, and carrier offsets incremented in 150 kHz steps until covering the whole range of powder spectral widths. About 8,000−30,000 transients were typically collected for each of these variable-offset experiments, with 50−100 ms recycle delays and 2 MHz spectral windows. All these acquisitions took place in a 11.75 T laboratory-built NMR spectrometer controlled by a Tecmag pulse programmer. Samples were packed on 7.5 mm containers and placed inside the coil of a home-built variable temperature static powder NMR probe providing up to 100 kHz *Rf* notation fields. Temperatures throughout all experiments were set with precooled/preheated gas streams using a custom-built controller; calibration of this system was based on the ^{1}H NMR signals of methanol and of ethylenglycol.[29] The chemical shift calibration of all these experiments was based on the $^{185/187}$Re NMR resonances of a saturated NH_4ReO_4 (aq.) solution, which in our spectrometer appeared at 113.8541 and 112.7180 MHz, respectively, with approximate widths of 8 kHz.

These ReO_4^- experiments were complemented with measurements on structurally analogous MnO_4^- groups. ^{55}Mn, a 100% abundant spin-5/2, was monitored on samples of $KMnO_4$, $CsMnO_4$, and PPh_4MnO_4. $KMnO_4$ and $CsMnO_4$ were obtained from Aldrich Chemicals and recrystallized from warm saturated aqueous solutions before analysis. PPh_4MnO_4 was prepared from a one-to-one reaction of PPh_4Cl (Aldrich) and $KMnO_4$ in warm water.[30] Most of the ^{55}Mn spectra were acquired on the laboratory-built 11.75 T solid-state NMR spectrometer and probe; spectra were also collected under MAS conditions at 4.7

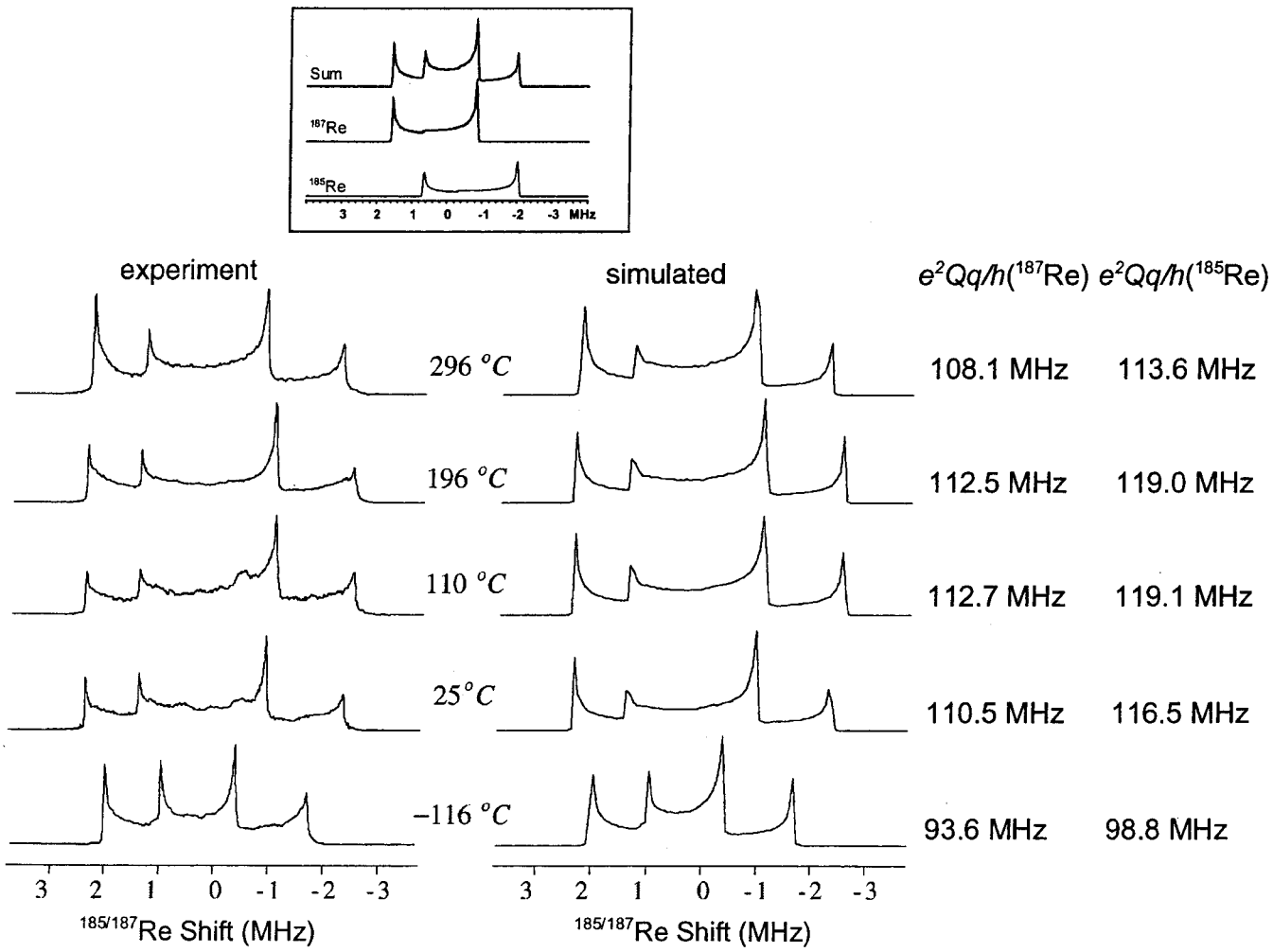

Figure 3. Experimental vs calculated wide-line $^{185/187}$Re NMR spectra of NH_4ReO_4, recorded as a function of the indicated temperatures, and simulated with the parameters shown. In all cases, the center frequency corresponds to 112.650 MHz. The top inset illustrates how the room-temperature line shape is made up of overlapping ^{185}Re and ^{187}Re NMR subspectra.

T using a laboratory-built variable-temperature spectrometer and probe system. ^{55}Mn NMR chemical shifts were referenced with respect to 0.1 M $KMnO_4$ (0 ppm), and both single-pulse and Hahn-echo experiments were carried out using 90° pulse widths of 3.5 μs and recycle delays of 0.5 s. Complementary static ^{75}As and ^{1}H NMR variable-temperature measurements were acquired at 11.75 T; the ^{75}As NMR spectra were referenced with respect to high-purity solid GaAs (0 ppm) obtained from Aldrich.

The simulation of the dynamic NMR spectra was carried out using custom-written C++ programs on a Dell Dimension 4100 733 MHz Parallel Pentium III computer. Hemispherical ZCW angle sets were used for powder averaging,[31] while the matrix diagonalization and inversion routines were performed with release 3.0 of the LAPACK linear algebra package.[32] Ab initio calculations of electric field gradients were conducted on the same computer using the Gaussian 98 program suite,[33] using the 6-311G* basis set for both restricted Hartree−Fock (RHF) and hybrid density functional methods (B3LYP).[34,35]

4. Results

Variable-Temperature Solid-State NMR of Perrhenates. Co-added frequency-swept $^{185/187}$Re static wide-line spectra collected for ammonium perrhenate as a function of temperature are pictured in Figure 3. A characteristic feature of these and other perrhenate spectra is the appearance of multiple singularities. These do not actually arise from multiple ReO_4^- sites in the lattice but from the two different Re isotopes being too close to be separately resolved. At the 11.75 T field used in our studies for instance, the solution state ^{185}Re and ^{187}Re Larmor frequencies are 112.72 and 113.85 MHz. This difference is consequently smaller than the central transition line widths observed for the isotopes in the solid, which are broadened into the 100s of kHz by the large rhenium nuclear quadrupole moments. Because the $^{185/187}$Re powder patterns overlap, they had to be simulated separately and summed together to retrieve the final spectrum (Figure 3, inset). This process is facilitated by the fixed ratios that a priori define the Larmor frequencies, quadrupole couplings and relative intensities of the overlapping powder patterns; no separate fitting of the two line shapes is thus necessary.

Ammonium perrhenate has actually been investigated in the solid state by a number of methods including neutron powder diffraction,[36,37] variable-temperature zero-field Re NQR,[38,39] and molecular dynamics simulations.[40] It crystallizes with a scheelite structure (tetragonal, space group $I4_1/a$)[41] and possesses no phase transitions between −269 and 127 °C. Its has, however, interesting thermal properties: the unit cell expands along the *c* axis and contracts along *a* with increasing temperature, keeping the unit cell volume constant. The *c*/*a* ratio of the unit cell starts increasing at approximately −150 °C, a feature that has been attributed to motions of the ammonium ions. These thermal

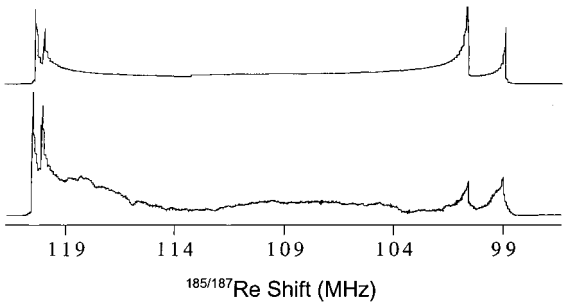

Figure 4. Experimental (bottom) vs calculated (top) wide-line $^{185/187}$Re NMR spectra of $NaReO_4$. Further details on the experiment and simulation parameters are given in the text.

anomalies may also be affecting the Re NMR spectra, which although not exhibiting dramatic line shape changes show an odd behavior. From room temperature up to ~300 °C, the EFG tensors are axially symmetric and relatively constant, and the values e^2qQ/h (^{185}Re) = 117.35 MHz and e^2qQ/h (^{187}Re) = 111.08 MHz that we obtain by NMR are in good agreement with those from the pure Re NQR experiments.[39] Yet as temperatures are lowered, the $^{185/187}$Re NMR spectra reveal a decrease in e^2qQ/h ($^{185/187}$Re), contrary to most variable-temperature trends for quadrupolar nuclei. On the basis of the molecular dynamics and variable-temperature neutron diffraction studies, it has been postulated that as temperature increases the N−H bond lengths in ammonia groups shorten, the H−N−H bond angles get smaller, and on average the N−H bonds stop pointing in an orderly manner toward the ReO_4^- oxygens. Thus, changes in the Re quadrupole coupling frequencies can be attributed to both intraionic structural changes as well as to interionic ammonium-perrhenate influences.

Another compound analyzed in this work was sodium perrhenate. $NaReO_4$ has been structurally characterized by single-crystal X-ray diffraction techniques and is also found to have a scheelite structure (tetragonal, space group $I4_1/a$),[42] similar to NH_4ReO_4 and to other metaperrhenates such as $KReO_4$ and $CsReO_4$. Previous NQR measurements on solid $NaReO_4$ revealed surprisingly large Re quadrupolar coupling constants for such symmetric group, e^2qQ/h (^{185}Re) = 300.02 MHz and e^2qQ/h (^{187}Re) = 283.91 MHz, with asymmetry parameters estimated ≤ 0.026.[38] Again, our $^{185/187}$Re NMR spectra conform to these values. Line-shape simulations of the $NaReO_4$ data reveal e^2qQ/h (^{185}Re) = 278 and e^2qQ/h (^{187}Re) = 268 MHz (Figure 4), representing some of the largest quadrupole coupling constants measured to date by solid-state NMR experiments. Due to the extreme spectral widths and long times associated with the acquisition of these powder patterns, variable-temperature experiments were not conducted on this sample.

Perhaps the most interesting of the Re compounds analyzed was tetraphenylarsonium perrhenate. $AsPh_4ReO_4$ is thought to have a different structure from the metaperrhenate scheelite structures above. A single-crystal X-ray diffraction study has not been conducted on this molecule; there are, however, a number of structurally analogous molecules which have been characterized by single-crystal and powder diffraction and which supposedly share the same crystallographic space groups and basic unit cell dimensions as $AsPh_4ReO_4$. Among these are the tetraphenylphosphonium, tetraphenylantimony, and tetraphenylbismuth perchlorates, whose single-crystal structures have all been determined, as well as the tetraphenylarsonium and tetraphenylphosphonium permanganates which were studied by powder diffraction.[43−45] All these salts show the same tetragonal space group $I\bar{4}$ and similar unit cell dimensions, as well as distorted XO_4^- tetrahedra possessing S_4 symmetry. It also follows from these structures that unlike in the scheelites, the ReO_4^- anions in $AsPh_4ReO_4$ are far removed from one another by large tetraphenylarsonium cations. Nevertheless, as was the case in the NH_4^+ and Na^+ compounds, only one crystallographic site should exist, and thus, only one resonance per isotope should be visible in the solid-state $^{185/187}$Re NMR spectrum.

Experimental $^{185/187}$Re variable-temperature wide-line NMR spectra of $AsPh_4ReO_4$ are presented in Figure 5A. It is seen that as the temperature drops from 296 to −90 °C, a conventional single-site spectrum showing an apparent increase in C_Q($^{185/187}$Re) is observed. Upon reaching ~−100 °C, however, the signal broadens and drops substantially into the noise, while on progressing downward to −160 °C, the emergence of two different rhenium sites becomes clearly visible. This low

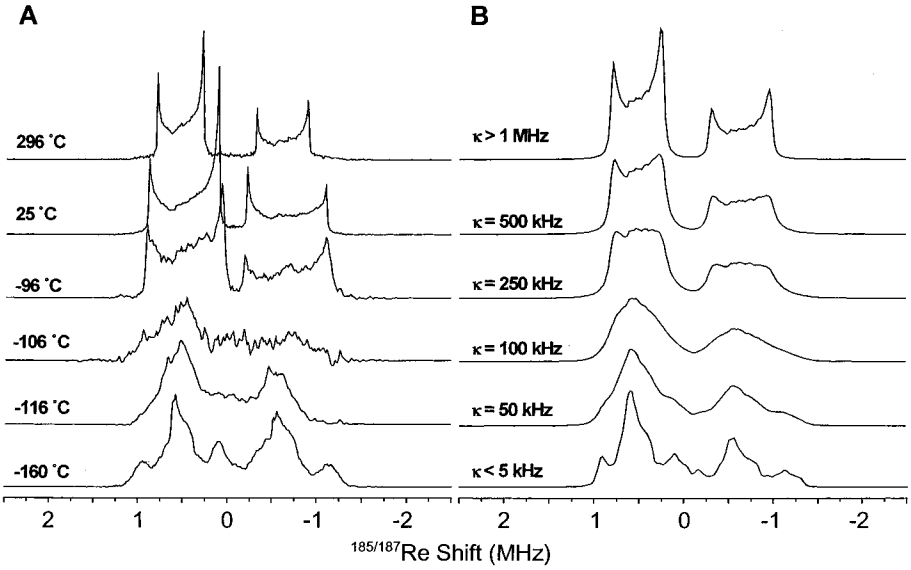

Figure 5. (A) Experimental variable-temperature $^{185/187}$Re wide-line NMR spectra of $AsPh_4ReO_4$ acquired at 11.75 T, with a center frequency of 112.65 MHz. (B) Best fit $^{185/187}$Re NMR spectra calculated using the model described in the text, the indicated exchange rates, and, for the sake of simplicity, temperature-independent coupling parameters. Intensity discrepancies between experiments and simulations near the coalescence regime are likely to arise from the fact that the former stem from an echo experiment, while the latter assume an ideal powder-wide excitation.

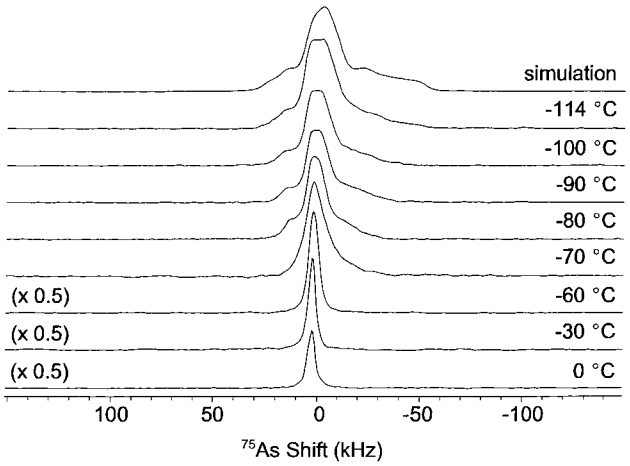

Figure 6. Variable-temperature static ^{75}As NMR spectra recorded for the central transition of $AsPh_4ReO_4$ at 11.75 T. The calculated low-temperature ^{75}As NMR spectrum on top was calculated assuming two inequivalent sites with couplings as provided in the text.

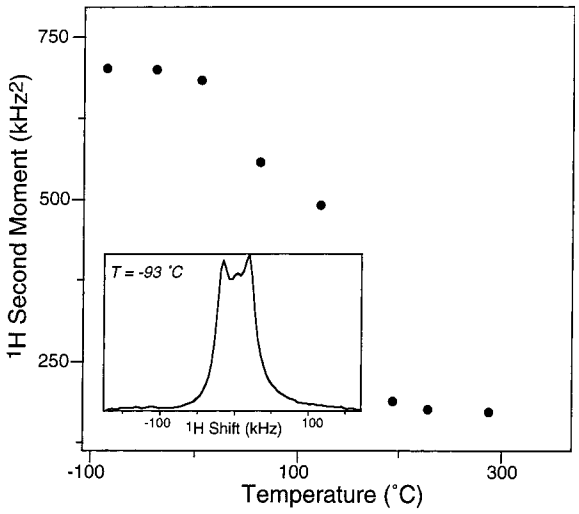

Figure 7. Variable-temperature ^{1}H second moments resulting from wide-line NMR spectra of $AsPh_4ReO_4$; the inset illustrates the line shape observed at the lowest temperatures using a 45° excitation pulse.

temperature spectrum can be simulated by overlapping subspectra arising from two equally populated Re sites with the following parameters: site 1, e^2qQ/h (^{185}Re) = 63.3 MHz, e^2qQ/h (^{187}Re) = 58.0 MHz, and η_Q = 0.15; site 2, e^2qQ/h (^{185}Re) = 31.6 MHz, e^2qQ/h (^{187}Re) = 29.0 MHz, and η_Q = 0.8.[46] We thus assign the spectra observed at and above room temperature to dynamically averaged quadrupolar powder patterns resulting from chemical exchange between two nonequivalent sites, with spectra at ~−100 °C representing the coalescence point.

Possible motions that come to mind upon considering how to analyze these rhenium variable-temperature spectra involve 2- and 3-fold reorientations about the nominal symmetry axes of the ReO_4^- tetrahedron, as well as a four-site exchange about the symmetry axes of this body. Yet a comparison with the numerical simulations reveals that none of these models can reproduce the experimental line shapes. In fact, an extensive search yielded the best-fit simulations shown in Figure 5B, involving an exchange between two sites whose EFG tensors are fixed with respect to an arbitrary molecular frame with the following angles: $(\alpha_1,\beta_1,\gamma_1)$ = (90°,90°,0°); $(\alpha_2,\beta_2,\gamma_2)$ = (0°,90°,0°). It is hard to rationalize such process if it is assumed that the central Re atom occupies the central S_4 position of the anion. Yet another challenge posed by the Re NMR relates to justifying the presence of two-site dynamics in a system where crystallographic data would indicate the existence of a single inequivalent chemical site. To further clarify these issues, we turned to two other NMR-active nuclei available in the sample: ^{75}As and ^{1}H.

There are very few reported instances of solid-state ^{75}As NMR in the literature, with some of the few examples being on rhombohedral arsenic and gallium arsenide metals.[47−50] Though ^{75}As is 100% naturally abundant, it is a spin-$^3/_2$ quadrupolar nucleus with a large quadrupole moment (0.29 barn), which usually results in very broad powder patterns. Static spin−echo ^{75}As NMR spectra of $AsPh_4ReO_4$, however, show narrow central transitions (Figure 6) with a single, slightly asymmetric Gaussian line shape ($\Delta\nu_{1/2} \approx$ 4600 Hz) at room temperature. As the temperature is lowered, however, spectra broaden, and below −80 °C, their NMR clearly reveals the presence of two chemically inequivalent sites. Simulations of the low-temperature spectrum yield the following parameters for them: site 1, e^2qQ/h (^{75}As) = 6.2 MHz and η_Q = 0.4; site 2, e^2qQ/h (^{75}As) = 2.9 MHz and η_Q = 0.5. Although these changes confirm the presence of two inequivalent sites as revealed by the $^{185/187}$Re NMR spectra, the two-site exchange model used to describe the latter's coalescence was not applied to the ^{75}As, as in this case, the second-order quadrupolar interactions were too similar to the natural line widths for a detailed treatment.

A valuable clue in the analysis of the $^{185/187}$Re data was also provided by variable-temperature wide-line measurements of the perrhenate's ^{1}H signals. Like in the case of the quadrupoles, these spectra reveal as well the onset of a chemically activated dynamics, as judged by the continuous line narrowing occurring above −30 °C (Figure 7). As the protons originating these signals are confined to the $[AsPh_4]^+$ groups and these are probably too large to undergo large amplitude reorientations or displacements, the narrowing is most likely stemming from a local motion of the phenyl groups, e.g., from rotations or π-flippings about their local para axes. The lattice changes brought about by these motions could in turn explain the coalescence processes reported by the ^{75}As and $^{185/187}$Re spin probes. Yet before putting forward a plausible model that accounts for the unusual features of the latter spectra (in particular, the multiple sites and their unusual 90° exchange angle), we turn to a summary of the dynamics observed in a structurally similar class of compounds.

^{55}Mn Static and MAS NMR of Permanganates. As a complement to the perrhenate studies, a survey of the potential dynamics that other XO_4^- groups may undergo in the solid phase was carried out. Targets of these studies included $KMnO_4$, $CsMnO_4$, and PPh_4MnO_4. $KMnO_4$ crystallizes in the orthorhombic *Pnma* space group, with four molecules per unit cell.[51] These permanganate ions do not have perfect tetrahedral point symmetry and are in fact composed of sets with different Mn−O bond distances: 1.622, 1.625, and 1.634. ^{55}Mn static and MAS NMR spectra of $KMnO_4$ have been reported in the literature;[52] a survey of their temperature dependence is pictured in Figure 8. At first sight, it may appear from the static ^{55}Mn NMR spectra that some sort of chemical exchange is taking place. ^{55}Mn MAS NMR, however, reveals that in fact the coupling parameters are simply changing continuously with temperature: these spectra can be simulated at 20 and −120 °C with e^2qQ/h = 1.65 MHz, η_Q = 0.3, and δ_{iso} = −7.0 ppm and e^2qQ/h = 1.95 MHz, η_Q = 0.25, and δ_{iso} = −14.5 ppm respectively, with a linear increase in e^2qQ/h and decrease in chemical shift for temperatures in between.

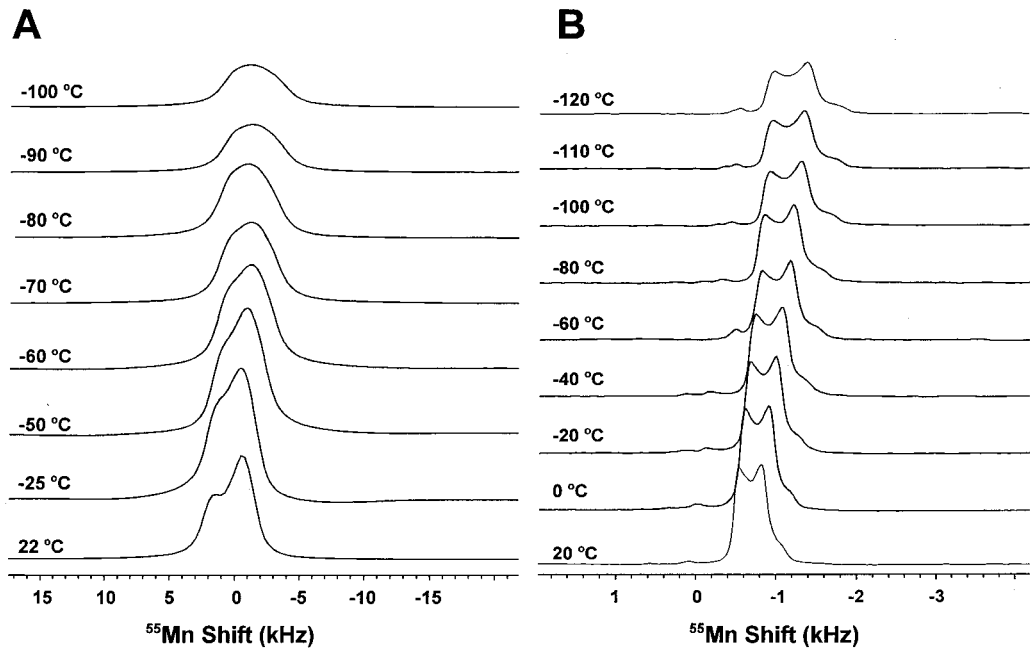

Figure 8. (A) Central transition static ^{55}Mn NMR spectra of $KMnO_4$ acquired at 11.75 T at the indicated temperatures. (B) ^{55}Mn MAS NMR spectra of $KMnO_4$ acquired at 4.7 T, illustrating the continuous variations of the central transition line shape upon changing temperature.

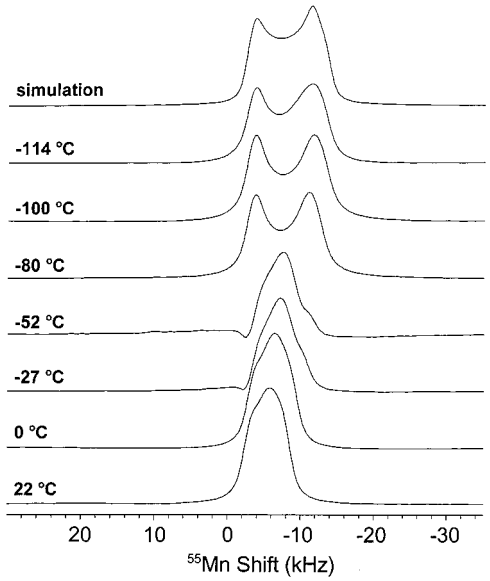

Figure 9. Static variable-temperature ^{55}Mn NMR spectra acquired for $CsMnO_4$ at 11.75 T. The bottom trace shows a central transition line shape calculated for the following coupling parameters: $e^2qQ/h = 6.8$ MHz, $\eta_Q = 0.15$, $\delta_{iso} = -47$ ppm, $\delta_{CS} = -18$ ppm, and $\eta_{CS} = 0.33$.

Although little is known about the NMR of cesium permanganate, the crystal structure of this salt has been determined and found to have the same space group (*Pnma*) as $KMnO_4$.[53] Mn−O bond lengths in $CsMnO_4$ range between 1.601 and 1.606 Å, and all O−Mn−O bond angles are different, meaning that also in this case the permanganate anion does not have perfect T_d symmetry. Also, as for $KMnO_4$, the static ^{55}Mn NMR spectra of $CsMnO_4$ reveal a slight temperature dependence of the metal's coupling parameters (Figure 9). Yet the line shapes also show distinct changes that cannot this time be solely explained in terms of continuous coupling changes. The ^{55}Mn MAS spectra (not shown) are also indicative of such dynamic exchange. The $CsMnO_4$ static line shape changes are in fact reminiscent of those presented in Figure 1 for various exchange models, even if insufficient spectral resolution in their features has hitherto prevented us from pinpointing the exact nature of the exchange.

Looking for further insight on the dynamics of $AsPh_4ReO_4$, we turned to the ^{55}Mn NMR of its analogue PPh_4MnO_4. Though no single-crystal data is available for this compound, both IR and X-ray powder diffraction suggest that tetraphenylphosphonium permanganate should be similar to the better characterized perchlorates.[30] The static room temperature ^{55}Mn NMR spectrum of this salt displays no significant second-order quadrupole broadenings; yet its classic spin-$^5/_2$ satellite pattern reveals a small quadrupole coupling $e^2qQ/h \approx 450$ kHz (Figure 10A). Upon lowering temperatures, the static central transition line shape broadens and shifts slightly, while the ^{55}Mn satellite transitions become distorted and indicate the presence of two sites below ca. −20 °C. More revealing perhaps, the ^{55}Mn MAS spectra of this compound clearly split at approximately −40 °C (Figure 10B),[54] while low-temperature 2D MAS exchange data reveals a dynamic interconversion occurring between two sites (Figure 10C). Although a comprehensive analysis of these MAS NMR line shapes remains to be done, it is evident that for both $AsPh_4ReO_4$ and PPh_4MnO_4 two inequivalent sites per unit cell are undergoing a thermally activated mutual interconversion.

5. Discussion

The main purpose of this work was to present a model for treating the effects of chemical exchange between N sites on the static NMR central transitions patterns arising from quadrupole nuclei, and then use such formalism to study the thermal behavior of XO_4^- groups in solids. Particular attention was focused on the solid-state NMR of $AsPh_4ReO_4$ and PPh_4MnO_4, which, according to preliminary expectations, should yield single sets of NMR resonances. Mutually exchanging sites were observed instead in both cases, which for $AsPh_4ReO_4$ could be ascribed to EFG tensors placed ∼90° apart from one another. This may at first sight seem surprising, as there is little in the symmetry of perrhenate groups that would suggest such relative orientations. To get further insight on the origins of this angle

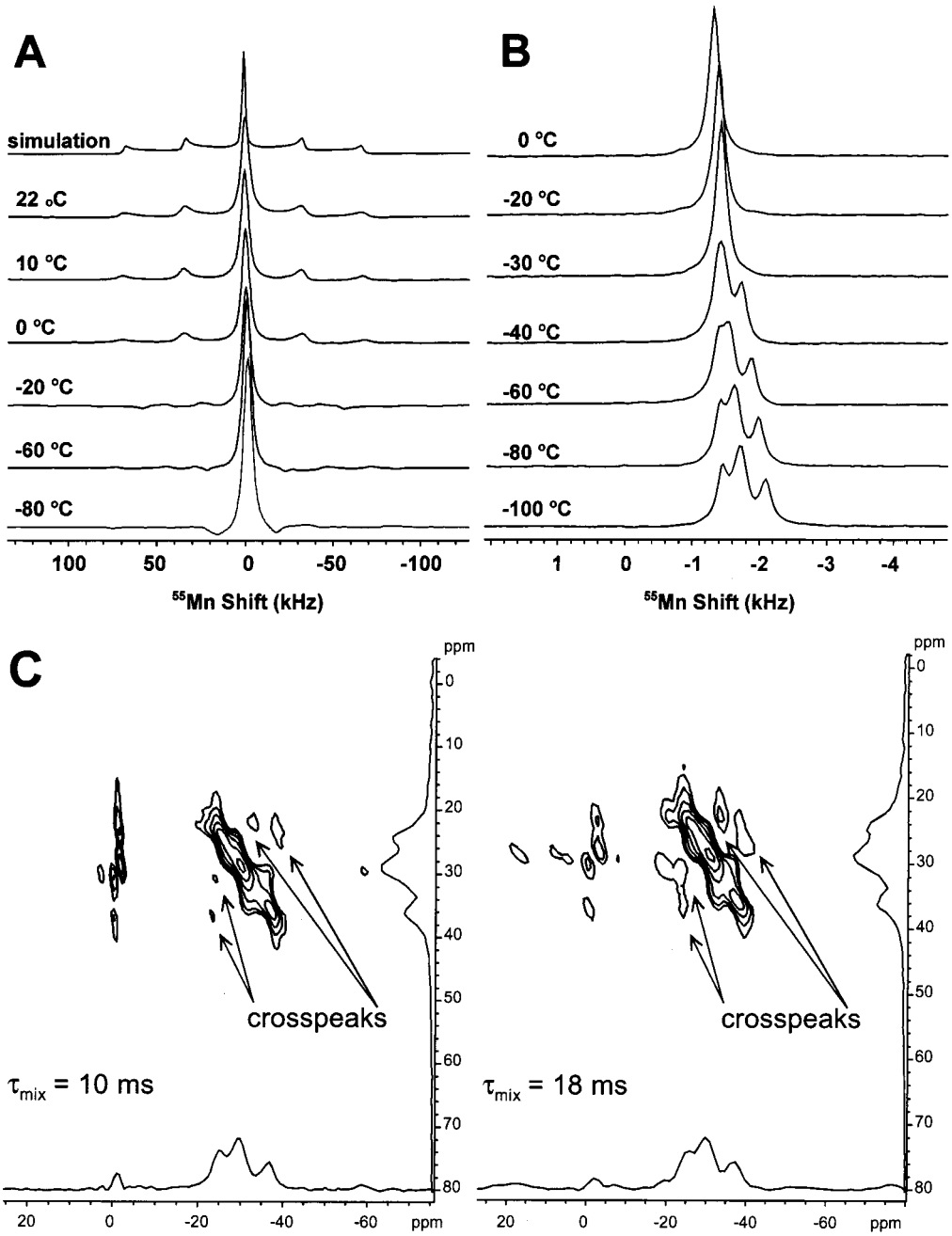

Figure 10. Experimental ^{55}Mn NMR spectra acquired for PPh_4MnO_4 under different conditions. (A) Static spectra showing the thermal evolution of the satellite transitions. Shown on top is the best fit simulation to a single site with $e^2qQ/h = 450$ kHz. (B) Central transition NMR spectra observed for the same compound undergoing MAS at 10 kHz; notice the line shape coalescence occurring between −60 and −30 °C, reminiscent to the one exhibited by each Re isotope in Figure 5. (C) 2D exchange MAS NMR spectra recorded for the central transition at −80 °C, revealing cross-peaks between two interconverting ^{55}Mn powder patterns.

as well as on the nature of the exchange process, ab initio calculations were implemented to pinpoint the approximate orientation of EFG tensors in distorted XO_4^- tetrahedra. To this end, we avoided XO_4^- groups possessing transition metals and focused instead on the lighter perchlorate anions, conducting the calculations using both restricted Hartree−Fock and hybrid density functional methods as a function of departures from an ideal tetrahedral symmetry. The orientations and magnitudes predicted by calculations for the ^{35}Cl EFG tensors of the crystallographically characterized perchlorate anions in PPh_4ClO_4 and $SbPh_4ClO_4$ are pictured in Figures 11A,B. On performing such calculations, we considered that chlorine atoms in these salts occupy sites of S_4 symmetry, implying that their anionic structures can be specified by one Cl−O bond length and two unique O−Cl−O angles (χ and ψ, Figure 11A). RHF/6-311G* calculations then show that as χ departs 109.5° e^2Qq/h follows in an almost linear fashion; yet in all cases, the largest component of the EFG tensor orients bisecting the angle χ. No 90° tensor reorientations such as those observed in the Re NMR experiments could therefore result from this type of distortion.

The main implication of these calculations is that the rhenium site in $AsPh_4ReO_4$ is probably not characterized by S_4 symmetry. Further EFG calculations on perchlorate groups reveal that upon departing from this type of symmetry, both the magnitudes and the orientations of this tensor's principal components become very sensitive to the arrangement of oxygen atoms about the chlorine. In fact, even minor deviations in one of the O−Cl−O bond angles (panels C vs D of Figure 11) can bring about 90°

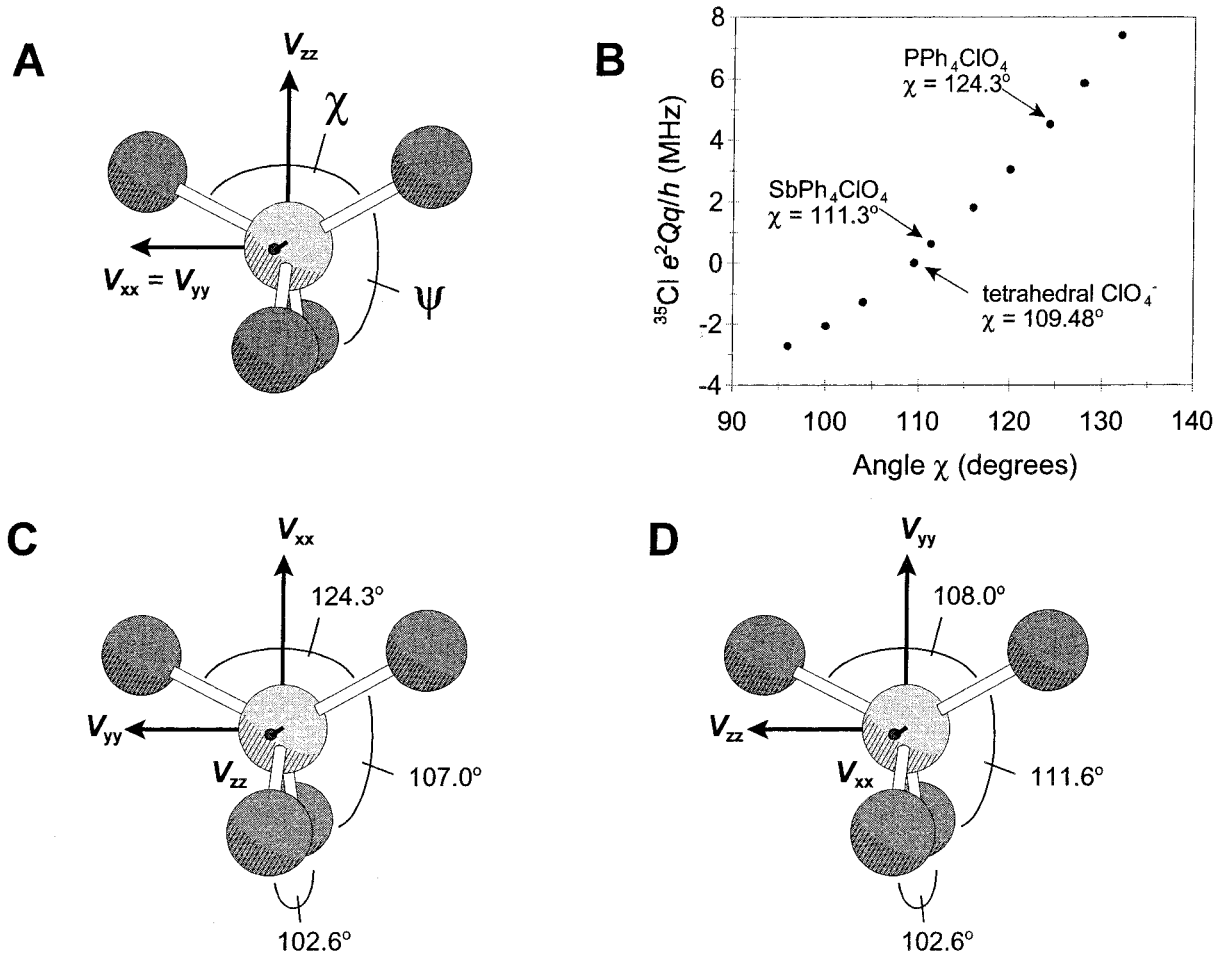

Figure 11. (A and B) RHF/6-311G* ^{35}Cl EFG tensor orientations and quadrupolar parameters calculated for the PPh_4ClO_4 and $SbPh_4ClO_4$ structures. The points in panel B reflect calculations based on these S_4 symmetry anions with r(Cl−O) fixed at 1.4 Å and a ^{35}Cl nuclear quadrupole moment of −0.083 barn, assuming solely a change in the χ angle. In all cases, an η_Q resulted 0. Panels C and D show the differing EFG orientations predicted by ab initio calculations for perchlorate geometries based on a lower C_{2v} symmetry (r(Cl−O) = 1.344 and 1.404 Å for the two pairs of oxygen, respectively). Subtle changes in geometry can then result in different EFG tensor orientations while yielding relatively constant quadrupolar parameters: $e^2Qq/h = -2.70$ MHz and $\eta_Q = 0.6$ in panel C; $e^2Qq/h = +2.70$ MHz and $\eta_Q = 0.2$ in panel D.

reorientations of the EFG tensors while leaving the actual quadrupolar coupling parameters e^2qQ/h and η_Q relatively constant. These are the kind of variations that had to be invoked for analyzing the $^{185/187}Re$ dynamic NMR data, suggesting that in fact mutual physical exchanges of perrhenate groups by 90° need not necessarily be happening in the solid. It is sufficient to assume minor thermally activated distortions in groups that are lacking S_4 symmetry, such as those which could arise for example from an onset of dynamics in the phenyl groups of the neighboring tetraphenylarsonia. These motions could average away inequivalencies between two distinct sites existing in the lattice at lower temperatures, while simultaneously explaining the thermal variations exhibited by the ^{75}As and ^1H NMR data.

6. Conclusions

The present work, together with the recent contributions of Farnan, Eckert, and co-workers, constitutes but first steps in a relatively underdeveloped area dealing with the application of half-integer quadrupolar NMR to the study of chemical exchange and dynamics in solids. From a spectroscopic standpoint, much remains to be done in the area of dynamic NMR on half-integer quadrupoles; this includes extending the present multisite formalism to other widespread time-dependent acquisition strategies such as MAS and multiple-quantum MAS, as well as modifying it for simultaneously accounting for all potential first- and second-order quadrupole effects in these experiments. From a chemical standpoint, it seems plausible that the advent of such new methods of NMR analysis will reveal a more dynamic nature for inorganic compounds and materials than was hitherto assumed, perhaps even akin to that which NMR has revealed for organic or biological solids.

Acknowledgment. We are grateful to Prof. C. Barnes (University Tennessee—Knoxville) for valuable discussions that triggered these studies, to Dr. A. Medek (Pfizer Pharmaceuticals) for initial assistance in the collection of the data, and to Prof. R. J. C. Brown (Queen's University, Canada) for helpful discussion on the thermodynamic behavior of metaperrhenates. This work was supported by the U.S. National Science Foundation through Grants DMR-9806810 and CHE-9841790 (Creativity Extension Award), by the U. S. Department of Energy through Grant 00ER15049, as well as by a Philip M. Klutznick Fund for Research (Weizmann Institute). L.F. is a Camille Dreyfus Teacher-Scholar (1996-2001).

References and Notes

(1) Spiess, H. W. *Dynamic NMR Spectroscopy*; Springer-Verlag: Berlin, 1978.

(2) Mehring, M. *High Resolution NMR in Solids*; Springer-Verlag: Berlin, 1983.

(3) Fyfe, C. A. *Solid State NMR for Chemists*; CFC Press: Ontario, 1983.
(4) Spiess, H. W. *Adv. Polym. Sci.* **1985**, *66*, 23.
(5) Schmidt-Rohr, K.; Spiess, H. W. *Multidimensional Solid-State NMR and Polymers*; Academic Press: London, 1994.
(6) McConnell, H. M. *J. Chem. Phys.* **1958**, *28*, 430.
(7) Abragam, A. *Principles of Nuclear Magnetism*; Oxford University Press: New York, 1961.
(8) Freude, D.; Haase, J. *NMR Basic Princ. Prog.* **1993**, *29*, 1.
(9) Vega, A. J. In *Encyclopedia of NMR*; Grant, D. M., Harris, R. K., Eds.; Wiley: New York, 1995; p 3869 and ff.
(10) Man, P. P. In *Encyclopedia of NMR*; Grant, D. M., Harris, R. K., Eds.; Wiley: New York, 1995; p 3838 and ff.
(11) Fitzgerald, J. *Solid State NMR of Inorganic Materials*; ACS Symp. Series, Vol. 717; Washington, DC, 1999.
(12) In *New NMR Techniques for Quadrupolar Nuclei*; Anderson, M. W., Duer, M. J., Eds.; Special issue Solid State NMR; 1999; Vol. 15.
(13) Smith, M. E.; vanEck, E. R. H. *Progr. NMR Spectrosc.* **1999**, *34*, 159.
(14) Cohen, M. H.; Reif, F. *Solid State Phys.* **1957**, *5*, 321.
(15) Das, T. P.; Hahn, E. L. *Nuclear Quadrupole Resonance Spectroscopy - Solid State Physics Supplement 1*; Academic Press: London, 1958.
(16) Maniv, S.; Reuveni, A.; Luz, Z. *J. Chem. Phys.* **1977**, *66*, 2285.
(17) Kristensen, J. H.; Farnan, I. *J. Chem. Phys.* **2001**, *114*, 9608.
(18) Witschas, M.; Eckert, H.; Freiheit, H.; Putnis, A.; Korus, G.; Jansen, M. *J. Phys. Chem. A* **2001**, *105*, 6808.
(19) Haeberlen, U. In *Advances in Mangetic Resonance, Supplement 1*; Waugh, J. S., Ed.; Academic Press: New York, 1976.
(20) However, when in an extreme narrowing regime with rates fast enough to average out the first-order quadrupolar couplings themselves, one can expect both tetrahedral jumps and/or MAS to yield isotropic resonances from half-integer quadrupole powders.
(21) Wooten, E. W.; Muller, K. T.; Pines, A. *Acc. Chem. Res.* **1992**, *25*, 209.
(22) Samoson, A.; Lippmaa, E.; Pines, A. *Mol. Phys.* **1988**, *65*, 1013.
(23) Harris, R. K.; Mann, B. E. *NMR and the Periodic Table*; Academic Press: New York, 1970.
(24) Klobasa, D. G.; Burkert, P. K. *Magn. Reson. Chem.* **1987**, *25*, 154.
(25) Grommelt, M.; Burkert, P. K. *Z. Naturforsch. B* **1989**, *44*, 1053.
(26) In *Transition Metal NMR Spectroscopy*; Pregosin, P. S., Ed.; Elsevier: Amsterdam, 1991.
(27) Massiot, D.; Farnan, I.; Gautier, N.; Trumeau, D.; Trokiner, A.; Coutures, J. P. *Solid State NMR* **1995**, *4*, 241.
(28) Medek, A.; Frydman, V.; Frydman, L. *J. Phys. Chem. A* **1999**, *103*, 4830.
(29) VanGeet, A. L. *Anal. Chem.* **1968**, *40*, 2227.
(30) Baran, E. J. *Anorg. Allg. Chem.* **1971**, *382*, 80.
(31) Eden, M.; Levitt, M. H. *J. Magn. Reson.* **1998**, *132*, 220.
(32) LAPACK is a Fortran 77 library providing routines for solving linear algebra problems. Code is available at http://www.netlib.org/lapack.
(33) Frisch, M. J. T., G. W.; Schlegel, H. B.; Scuseria, G. E.; Robb, M. A.; Cheeseman, J. R.; Zakrzewski, V. G.; Montgomery, Jr., J. A.; Stratmann, R. E.; Burant, J. C.; Dapprich, S.; Millam, J. M.; Daniels, A. D.; Kudin, K. N.; Strain, M. C.; Farkas, O.; Tomasi, J.; Barone, V.; Cossi, M. *Gaussian 98*; Gaussian Inc.: Pittsburgh, PA, 1998.
(34) Becke, A. D. *J. Chem. Phys.* **1993**, *98*, 5648.
(35) Lee, C.; Yang, W.; Parr, R. G. *Phys. Rev. B* **1998**, *37*, 785.
(36) Brown, R. J. C.; Shortreed, M. E.; Szabo, A. J.; Powell, B. M.; Stuart, S. N. Z. *Z. Naturforsch.* **1992**, *47A*, 308.
(37) Powell, B. M.; Brown, R. J. C.; Harnden, A. M. C.; Reid, J. K. *Acta Crystallogr.* **1993**, *B49*, 463.
(38) Burkert, P. K.; Eckel, M. F. *Z. Naturforsch.* **1973**, *28B*, 5.
(39) Szabo, A. J.; Brown, R. J. C. *Z. Naturforsch.* **1993**, *49A*, 302.
(40) Brown, R. J. C.; Lynden-Bell, R. M. *J. Phys. Condens. Matter* **1994**, *6*, 9903.
(41) Kruger, G. J.; Reynhardt, E. C. *Acta Crystallogr.* **1978**, *B34*, 259.
(42) Atzesdorfer, A.; Range, K.-J. *Z. Naturforsch.* **1995**, *50B*, 1417.
(43) Bordner, J.; Freedman, L. D. *Phosphorous* **1973**, *3*, 33.
(44) Ferguson, G.; Glidewell, C.; Lloyd, D.; Metcalfe, S. *J. Chem. Soc., Perkins Trans. 2* **1988**, 731.
(45) Vittal, J. J.; Dean, P. A. W. *Acta Crystallogr.* **1996**, *C52*, 3185.
(46) As for the remaining perrhenates and due to the dominant role played by second-order quadrupolar interactions on Re NMR powder patterns, the effects of chemical shielding anisotropy could not be assessed for this compound.
(47) Potter, L. D.; Wu, Y. *J. Chem. Phys.* **1995**, *103*, 4834.
(48) Pietrass, T.; Bifone, A.; Krueger, J.; Reimer, J. A. *Phys. Rev. B: Condens. Matter* **1997**, *55*, 4050.
(49) Taylor, P. C.; Hari, P.; Kleinhammes, A.; Kuhns, P. L.; Moulton, W. G.; Sullivan, N. S. *J. Non-Cryst. Solids* **1998**, *227*, 770.
(50) Bastow, T. J. *J. Phys. Condens. Matter* **1999**, *11*, 569.
(51) Palenik, G. J. *Inorg. Chem.* **1967**, *6*, 503.
(52) Burton, D. J.; Harris, R. K. *J. Chem. Soc., Chem. Commun.* **1982**, 256.
(53) Hoppe, R.; Fischer, D.; Schneider, J. *Z. Anorg. Allg. Chem.* **1999**, *625*, 1135.
(54) The lower temperatures at which these second-order line shape changes occur vis à vis the first-order line shape changes are consistent with the longer time scales of the former interactions.